Carbon 156 (2020) 1–9

Contents lists available at ScienceDirect

Carbon

journal homepage: www.elsevier.com/locate/carbon

Oxygen reduction reaction: Semi-empirical quantum mechanical and electrochemical study of Printex L6 carbon black

Paulo Jorge Marques Cordeiro-Junior [a, *], Roger Gonçalves [b], Thais Tasso Guaraldo [a], Robert da Silva Paiva [b], Ernesto Chaves Pereira [b], Marcos Roberto de Vasconcelos Lanza [a, **]

[a] São Carlos Institute of Chemistry, University of São Paulo, Avenida Trabalhador São-Carlense 400, São Carlos, SP, 13566-590, Brazil
[b] Department of Chemistry, Federal University of São Carlos, São Carlos, SP, 13565-905, Brazil

ARTICLE INFO

Article history:
Received 3 June 2019
Received in revised form
10 September 2019
Accepted 11 September 2019
Available online 12 September 2019

Keywords:
Printex L6 carbon black
Quantum mechanical semi-empirical calculations
Electrochemical characterization

ABSTRACT

Amorphous carbon black (CB) is a highly reactive material for O_2 reduction and widely employed in H_2O_2 generation. Most studies published have confined their investigation to few electrochemical properties of CB and its morphological and structural characterization. However, an in-depth understanding of CB properties and their effects on oxygen reduction reaction appears to be the key to making significant progress in this field. This paper describes the use of quantum mechanical semi-empirical calculations to obtain structural information and electrochemical impedance spectroscopy to access the electrochemical information of Printex L6 CB (PCL6). It is the first report of its kind in the literature. The semi-empirical results show that PCL6 electrode presents an increase in the number of hotspots due to the presence of large amount of sp^2 carbon and functional groups in its composition, which favors O_2 adsorption at lower potentials. The equilibrium distance on PCL6 electrode is closer to the distance of a double bond (C=O), reinforcing O_2 bridge-like adsorption model. Furthermore, PCL6 had proved to be thermodynamically more favourable to O_2 adsorption and requires relatively lower energy and potential (shift of 150 mV). PLC6 is found to undergo an activation process, probably associated with O_2 adsorption, prior to the beginning of reaction.

1. Introduction

Oxygen reduction reaction (ORR) has drawn considerable attention among researchers in the field due to its complexity and relevance in different electrochemical devices. Two different products can be generated via ORR depending on the dominant pathway employed. In acid medium, oxygen can be reduced on the cathode surface, forming hydrogen peroxide (H_2O_2) via the two-electron mechanism (Eq. (1)). The H_2O_2 generated can be further reduced to H_2O through the transfer of two extra electrons or oxidized back to O_2 (Eqs. (2) and (3)). Oxygen can also undergo complete reduction to H_2O through the direct consumption of four electrons (Eq. (4)) [1,2].

$$O_2 + 2\,H^+ + 2\,e^- \rightarrow H_2O_2 \qquad \left(E^0 = 0,682\ \text{V vs SHE}\right) \tag{1}$$

$$H_2O_2 + 2\,H^+ + 2\,e^- \rightarrow 2\,H_2O \qquad \left(E^0 = 1,770\ \text{V vs SHE}\right) \tag{2}$$

$$H_2O_2 \rightarrow 2\,H^+ + 2\,e^- + O_2 \tag{3}$$

$$O_2 + 4\,H^+ + 4\,e^- \rightarrow 2\,H_2O \qquad \left(E^0 = 1,229\ \text{V vs SHE}\right) \tag{4}$$

The most efficient electrocatalysts employed in ORR via the four-electron mechanism are usually composed of platinum and its alloys [3,4]. In view of that, these materials are widely used as cathode in fuel cells. On the other hand, carbon nanomaterials have demonstrated high selectivity in terms of hydrogen peroxide

* Corresponding author.
** Corresponding author.
E-mail addresses: pjmcjunior@usp.br (P.J.M. Cordeiro-Junior), marcoslanza@usp.br (M.R.V. Lanza).

https://doi.org/10.1016/j.carbon.2019.09.036
0008-6223/

formation as can be observed in equation (1) [5]. Taking that into consideration, studies in this area have been directed toward understanding and developing highly efficient low cost electrocatalysts. Carbon black comprises a class of materials that present different properties depending on the synthesis route applied [6]. Amorphous carbon black presents high catalytic activity for ORR via two electrons and, consequently, for the electrogeneration of H_2O_2. Accordingly, these materials can be applied in advanced oxidation processes (AOP) for wastewater treatment [7,8]. Among carbon black matrices, Printex L6 carbon black (PCL6) has become widely popular because of its great surface area and the presence of significant amount of oxygenated functional groups, such as quinones, anthraquinones, carboxylic acids, to name a few, in its composition [8].

Yeager et al. [1,2] have shown that carbon black or graphite electrodes can generate H_2O_2 via an in-depth interaction between O_2 with the oxygenated functional groups on carbon surface. Based on the mechanism proposed by these researchers, O_2 binds strongly to a carbon lying close to the carbonyl group, leading to the formation of superoxide O_2^- species, which, in acid medium, react with H^+, leading to the formation of H_2O_2 [1,9]. The presence of functional groups in carbon black can be determined through the application of Fourier transform infrared attenuated total reflection spectra (ATR-FTIR) technique [8].

Mechanical-quantum calculations are very useful in the sense that they help one to understand processes at the atomic level. Although ab initio methods are the most widely used technique in the field, semi-empirical methods are still useful when it comes to investigating adsorption, desorption and energies involved in such processes [10]. In addition, semi-empirical methods also allow one to predict the behaviour of materials on electrode surfaces. Although theoretical studies involving H_2O_2 formation reaction have already been explored in the literature [11], there are no studies in the literature involving catalytic reactions on carbon black substrates.

The electrochemical properties of carbon-based materials are usually investigated by voltammetric experiments. The use of rotating disk electrode (RDE) or rotating ring-disk electrode (RRDE) techniques allows one to obtain steady state polarization curves, which lead to the ORR pathway. These electrochemical assays may be useful for evaluating the ORR mechanism. Both RDE and RRDE techniques are used under hydrodynamic conditions. The products generated are directly transported to the ring; and through the application of fixed biased potential, one can detect the presence of only H_2O_2. Furthermore, using the correlation between the disk and the ring currents, one can measure the H_2O_2 produced and have a better understanding of the mechanism pathway [1]. The ORR mechanism has been extensively studied with the aim of determining the number of electrons consumed in the process.

Electrochemical studies conducted on carbon black have included investigating differences in the current distribution profile [7] and material selectivity toward H_2O_2 production using scanning electrochemical microscopy (SECM) [8,12]. In this sense, in order to meet all these requirements for hydrogen peroxide evolution, a better understanding of the materials properties is seen to be vital if one is to make significant advances in the field.

Among the electrochemical techniques widely reported in the literature, impedance spectroscopy (EIS) has been shown to be a powerful technique when it comes to obtaining mechanistic information on relevant materials under investigation [13–15]. However, most researchers have confined the use of this technique to the determination of charge transfer resistance [15]. For instance, gas diffusion electrodes prepared using a mixture of carbon black and active carbon have been characterized by ORR [15]. Similarly, $Pt/TiO_2/C$ and $Pt/SnO_2/C$ catalysts have been investigated using EIS [13]. Bera et al. [14] reported to have used the ORR mechanism for the production of water ($4e^-$) in alkaline solution using EIS for a series of N-doped Vulcan electrodes.

To the best of our knowledge, there are no reports in the literature regarding a comprehensive mechanistic study conducted using electrochemical impedance spectroscopy for unmodified Printex L6 carbon black. Clearly, a detailed study of this nature would significantly contribute to advances in the area of hydrogen peroxide electrosynthesis and in the application of PCL6 in fuel cells, supercapacitors and batteries, as well as in advanced degradation processes of pollutants. In this context, this work sought to characterize Printex L6 (PCL6) carbon black, and quantum mechanical semi-empirical calculations were used to obtain structural information on this material. The use of semi-empirical calculations in order to obtain structural information of a given material is one of the novel contributions of this work. Electrochemical properties were investigated using conventional voltammetric studies and electrochemical impedance spectroscopy considering different mass and/or charge transfer regions. The oxygen reduction reaction on PCL6 electrode was compared to that of glassy carbon substrate in terms of H_2O_2 evolution.

2. Experimental

2.1. Electrode preparation

The RRDE electrode used in the experiments was previously polished with 0.3 and 0.05 μm alumina polishing powder. Thereafter, the electrode was subjected to ultrasonic bath in isopropyl alcohol and ultrapure water for 5 min each. The PCL6 material was thermally treated at 120 °C for 24 h prior to use. A suspension was prepared by dispersing 1 mg of PCL6 powder in 1 mL of ultrapure water and sonicated for 15 min using Soni-Tech ultrasonic bath model TOP404A. 25 μL of PCL6 solution from the previously prepared suspension were placed on a glassy carbon plate and dried under N_2 stream at 1.0 mL min^{-1} (1 h).

2.2. Electrode characterization

The morphologies of the PCL6 and glassy carbon substrates were characterized by scanning electron microscopy (FEG-SEM) and X-ray energy dispersive spectroscopy (EDS) using FEI Company equipment model Inspect F50. The electron beam energy applied was 10 keV. The size distribution profile of the images was obtained through the application of the software Image J. The transmission electron microscopy (TEM) analysis was performed using JEOL JEM-2100 electron microscope operating at 200 kV. Carbon-coated copper grids were used to immobilize the diluted PCL6 suspensions, allowing the slow evaporation of the solvent at room temperature. The Brunauer-Emmett-Teller (BET) surface area and the Barrett-Joyner-Halenda (BJH) pore size distribution were measured by nitrogen adsorption/desorption isotherms at −196 °C using Micromeritics ASAP 2420.

Electrochemical characterization was performed in a three-electrode electrochemical cell, which consisted of RRDE working electrode from PINE Instruments (0.2476 cm^2 disk area and 0.1866 cm^2 ring area), Pt counter electrode, and Ag/AgCl reference electrode (3 M KCl). The RRDE experiments were performed using Metrohm Autolab model PGSTAT-128 N potentiostat. Cyclic and linear voltammetry analyses were conducted using an aqueous electrolyte containing 0.1 mol L^{-1} K_2SO_4, under pH of 2.5, adjusted with H_2SO_4. The electrolyte was previously purged with N_2 or O_2, and the gas flow was maintained during the experiment. The potential range of +0.4 to −0.8 V was applied to the RRDE disk at $v = 5$ mV s^{-1}; the ring potential was kept constant at +1.0 V. The

electrode rotation was also kept constant at 900 rpm.

The electrochemical impedance spectroscopy measurements were carried out using a three-electrode electrochemical configuration. A bare glassy carbon rotating disk electrode and PCL6 modified electrode were used as working electrodes. The data were collected at a rotation of 900 rpm during the measurements. The data were registered at 10 points per decade from 10 kHz to 10 mHz with AC perturbation of 10 mV. The experiments were performed in the presence of saturated N_2 or O_2 gases to aid our analysis and understanding of the behaviour of each electrode. The *dc* potentials of −0.8, −0.6, −0.4, −0.3, −0.2, −0.1, 0, +0.1 V were applied after the voltammetric experiments. All electrochemical experiments were performed in Autolab potentistat/galvonostat (PGSTAT-128 N) using the FRA32 M module.

2.3. Computational quantum-mechanical calculation

The theoretical experiments were carried out using MOPAC2016 semi-empirical software [16] with Hamiltonian PM7 [17]. The structures were built in Gabedit 2.5.0 [18], which was also used as structure viewer. The PCL6 structure was designed based on the studies published in the literature [2]; the structure is similar to that of graphene sheets assembled in several layers, as such, graphene folders were drawn to simulate the surface of PCL6. Considering that glassy carbon (GC) does not present a crystalline structure, *i.e.*, it is amorphous, its structure was developed based on the glass structure using sp^3 and sp^2 carbon and without long-range ordering. In both PCL6 and GB structures, the high reactive open-shell carbon atoms were saturated with hydrogen atoms. Although this strategy has no effect on the general properties of the substrates, the approximation helps the convergence of the properties of the material.

Both structures were subjected to relaxation using the AMBER 99 (Assisted Model Building with Energy Refinement) Molecular Dynamics (MD) package implemented in Gabedit [19]. The relaxation occurred for 10 ps (long enough for a solid material) at 300 K, and the atomic trajectory was calculated using the Verlet Velocity algorithm [20]. Finally, optimization was performed at semi-empirical level using PM7 aiming at obtaining the most stable structure. Subsequently, using the O_2 molecule as probe, a 20 × 20 nm solvent-accessible surface area of each sample was scanned in order to find a heat-map of O_2 adsorption sites on the substrates. The next step involved the scanning of a z-axis in an adsorption site so as to verify the strength and length of O_2 adsorption. The distance considered in the z-axis was long enough to prevent any interaction between the O_2 molecule and the substrate; subsequently, this distance was decreased systematically in order to find the interaction energy of the system. The non-interacting energy was defined as zero. All the calculations were carried out in the presence of water simulated as a continuum solvent, modelled by COSMO (conductor-like screening model) [21].

3. Results and discussion

3.1. Morphological and structural characterization

The morphological and structural characterization was performed through the comparison of the glassy carbon substrate with the Printex L6 carbon black (PCL6). FEG-SEM micrographs (Fig. 1A and B) and EDX (Fig. 1D) analyses were conducted for both samples. The particle size distribution (Fig. 1E) and TEM images (Fig. 1C) of the PCL6 sample were also subjected to characterization.

The PCL6 film exhibited a highly porous morphology with particle aggregation on the film surface. In spite of the particle agglomeration, the mean size of the particle was 35 nm (C). EDX analysis showed that the amount of oxygen present in the amorphous carbon matrix was around 3.6% (D); this implies the existence of oxygenated functional groups on the carbon surface, which is in agreement with the literature [1,2].

The concentration of carbon and oxygen was determined by elemental analysis and XPS (C 1s and O 1s spectra) in our previous work [12,22]. PCL6 is mainly composed of 92.3% of carbon and 7.7% of oxygen. Nitrogen is also present at significantly lower levels (>0.2%). The presence of oxygen considerably improves the electrocatalytic activity of carbon nanomaterials. This behaviour was confirmed by comparing the electrocatalytic activity of PCL6 and Vulcan XC72R with different oxygen levels [22]. C1 s spectra revealed the presence of aliphatic (284.5 eV) and aromatic (285.4 eV) hydrocarbons related to graphitic carbon and sp^3 C, respectively. The hydrocarbons also contained oxidized species (sp^2) including carboxylic, carbonylic and O−C groups at 289.3, 287.8 and 286.3 eV. The aromaticity of the carbon structure was confirmed by the presence of the peak at 291.0 eV. The presence of oxygen species was also confirmed by O1s core level spectra at 531.8 (O═C), 532.5 (O−C) and 533.8 eV (O−C═O). The additional peak observed at 535 eV has been shown to indicate the presence of molecular water [22].

The amorphous feature of PCL6 was confirmed by X-ray diffraction analysis [12,23] (data not shown). Broad reflections were determined at approximately 2θ 24.7° and 43.5° [12].

PCL6 exhibits a typical type-IV isotherm with H1 hysteresis loops at $P/P_0 > 0.8$ (Fig. 2A); this shows that it is a porous material known to form agglomerates or approximately uniform spheres. With the aid of BJH and BET adsorption analyses, the pore size distribution was found to show a large peak ranging from 20 to 50 nm, with a maximum value at 37 nm (value close to that obtained via SEM analysis). The surface area and pore volume obtained were 295.35 $m^2 g^{-1}$ and 0.564 $cm^2 g^{-1}$, respectively.

3.2. Semi-empirical quantum mechanical calculation

As aforementioned, an oxygen molecule was used as probe in order to obtain the energy surface of each simulated substrate. Fig. 3 shows the energy profile when O_2 is at fixed distance from the electrode. In the case of the vitreous carbon, one will observe that certain regions present negative energies, while a greater part of the regions shows no energetic gain; this means that adsorption does not occur spontaneously. This finding implies that little additional energy is required for adsorption to occur. In the case of PCL6, the presence of a great amount of sp^2 carbons leads to the generation of several hotspots with high adsorption energy. These underlying differences observed between the GC and PCL6 means that the reaction rate on PCL6 will be faster than on GC due to the higher density of active sites found on PCL6. In addition, due to higher adsorption energy of PCL6, the reaction on this material is expected to occur at lower overpotentials.

Fig. 3C shows the energy profile when O_2 molecule approaches the electrode surface, coming from a distance far enough to the point of impeding any interaction with the sample (i.e. coming from the bulk of the solution). The equilibrium distance on PLC6 (1.48 Å) is similar to that of C═O bond (1.44 Å). The values calculated here have important consequences once O_2 is expected to undergo a bridge-like adsorption [24]. In this sense, the distance could indicate a resonance situation, in which oxygen and carbon atoms participate in the reaction. In the case of GC, the equilibrium distance (1.93 Å) is found to be greater than the typical bond distance [24]; this implies that there is solely an electrostatic interaction between the adsorbate and the substrate. Furthermore, the width of the energy also suggests a diffuse interaction with the GCE. Thus, since the strength of the substrate-adsorbate interaction is a key

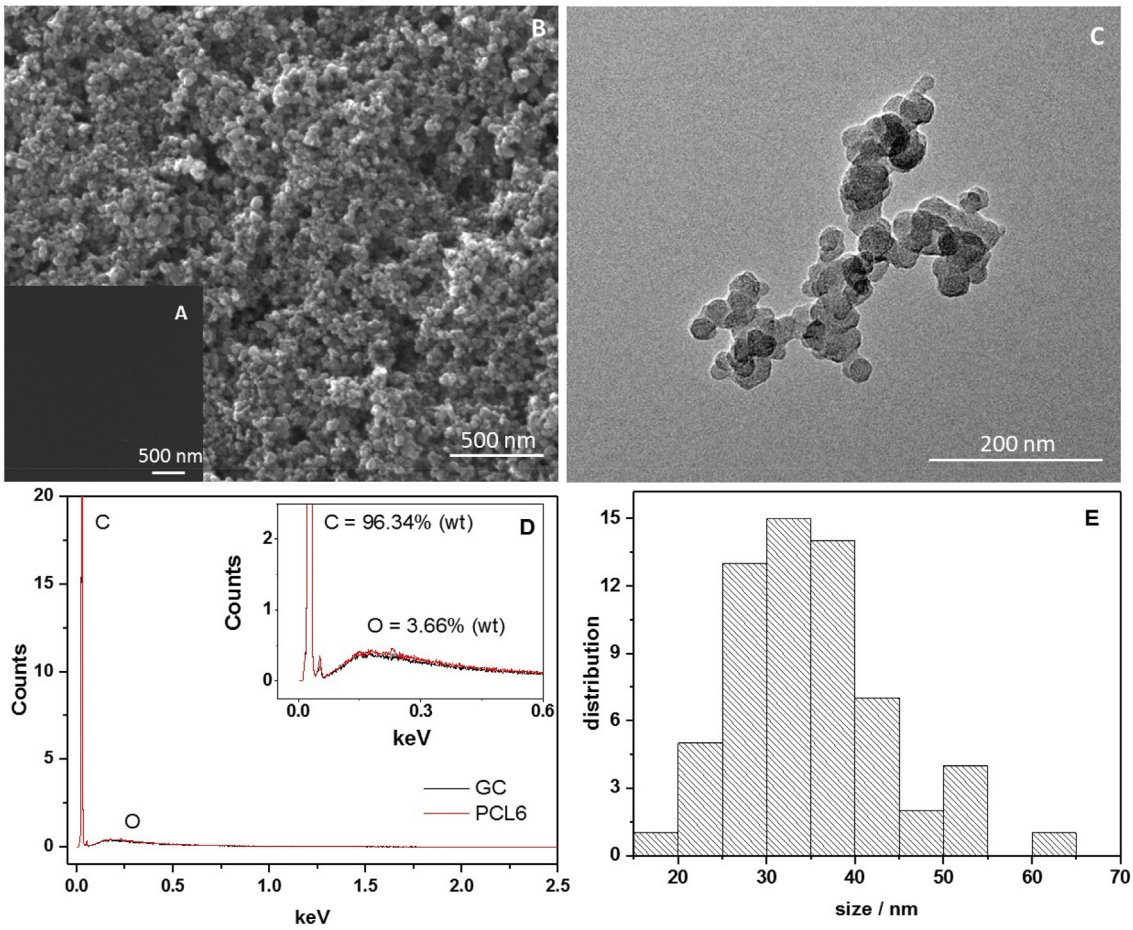

Fig. 1. FEG-SEM micrographs for GC (A) and PCL6 (B) samples and the respective EDX spectra (D) for GC (black line) and PCL6 (red line). TEM analysis (C) and particle size distribution (E) for PCL6. (A colour version of this figure can be viewed online.)

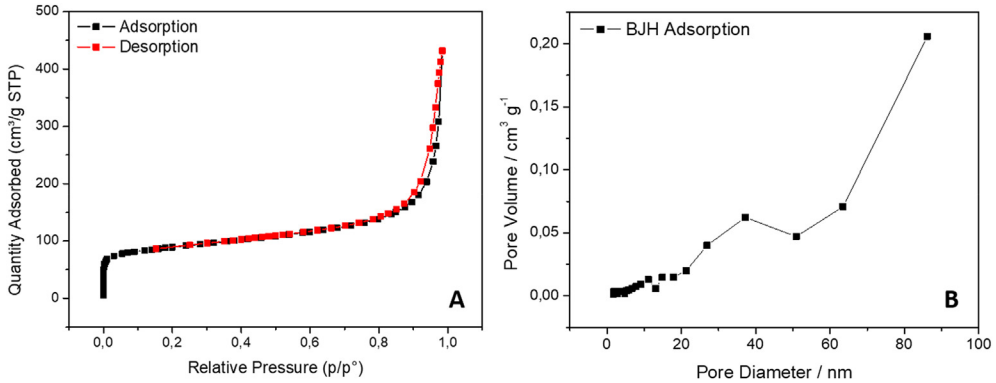

Fig. 2. Brunauer-Emmett-Teller (BET) isotherm (A) and Barrett-Joyner-Halenda (BJH) pore size distribution (B) for PCL6.

determinant of catalytic reaction, a stronger catalytic effect on the PCL6 is expected [25,26].

The bond distance and energy of interaction were also calculated taking into account the atom substituent in the vicinal carbon, where O_2 is bonded. First, one will notice that substituent groups that remove electronic density (i.e. being more electronegative than carbon sp^2) increase the binding energy of the adsorbate, suggesting an improvement in the catalytic effect. As described in the literature [1,2], among these substituents, the **=O** group presents interaction energies more effectively, slightly close to the carboxylic group. On the other hand, the **-OH** group leads to a worsening of the calculated values.

Fig. 3E and 3F shows the partial charge distribution, obtained by Mulliken charges, in the two simulated situations. The surface colour depends on the partial charge on each element. One can clearly observe that the GC surface is characterized by an electrostatic interaction, since O_2 molecule has a negative partial charge (light green colour), while carbon atoms have a positive charge (cyan colour). By contrast, the partial charge distribution on PCL6 shows that, close to the adsorbed O_2, the charge is slightly positive;

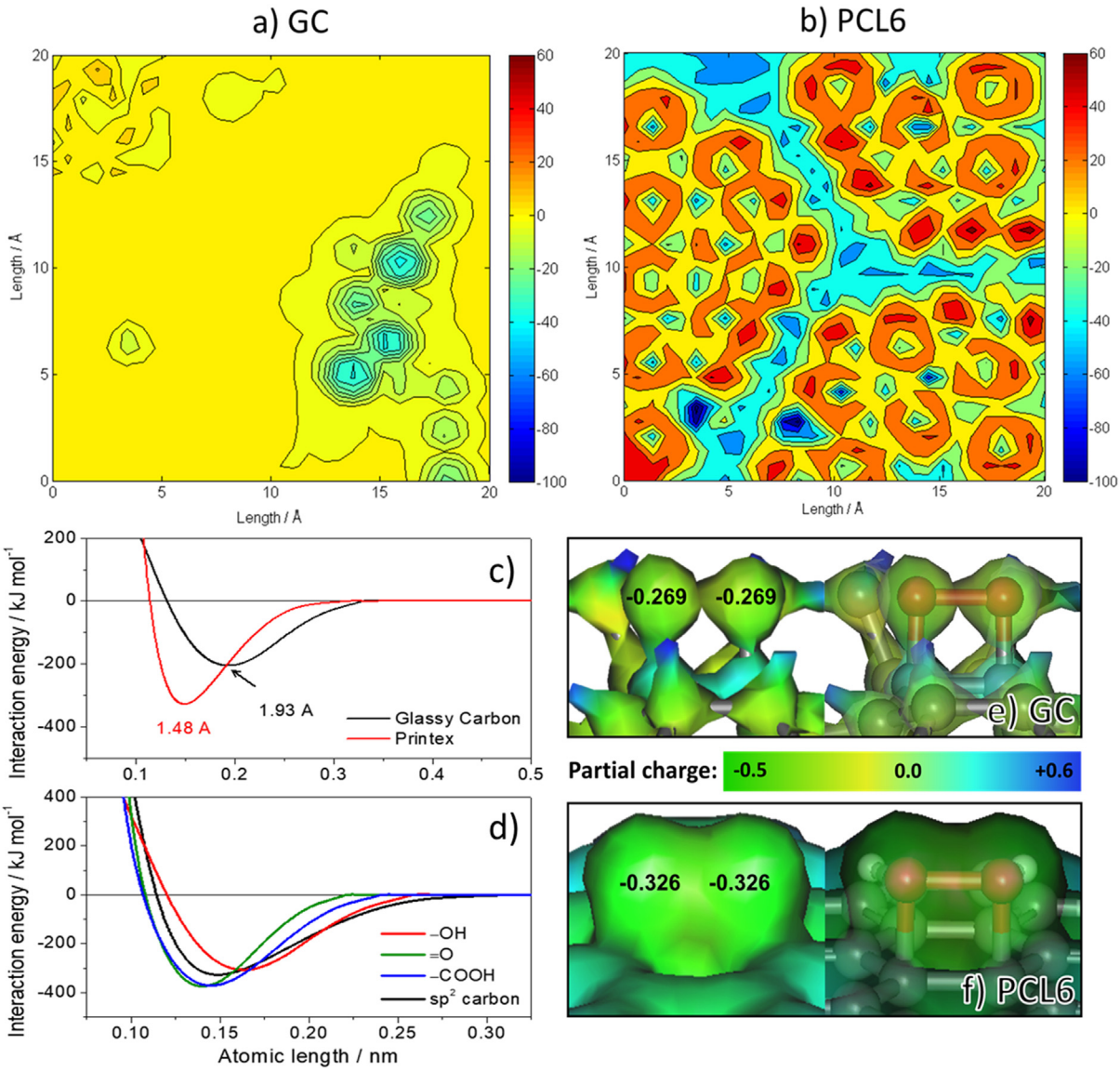

Fig. 3. O_2 adsorption energy surface for (A) GC and (B) PCL6, (C) and (D) equilibrium atomic length energy curve and Mulliken partial charges along with electron density surface in the region around O_2 adsorbed on (E) GC and (F) PCL6. (A colour version of this figure can be viewed online.)

this ensures the stabilization of the negative partial charge of both O_2 and carbon atoms that are bonded to PCL6. Finally, the charge distribution surface reinforces the existence of a resonance condition, since the surfaces are distributed throughout the formed ring and have the same partial charges (−0.326).

3.3. Electrochemical characterization

Electrochemical assays by linear scanning voltammetry with RRDE were performed using PCL6 micro-layer placed on the disk (Fig. 4A) at different rotation rates: 100; 400; 900; 1600 and 2500 rpm. The currents measured on the disk are related to ORR and coupled reactions, such as hydrogen reduction reaction. A constant potential of +1.0 V was applied on the RRDE ring. The current detected stemmed from H_2O_2 oxidation only, since this current potential was not positive enough to promote H_2O oxidation. The ORR contribution via $2e^-$ was found to be significant on the PCL6 electrode. The CV presents three distinct regions. In the first region, spanning between +0.4 and −0.1 V, only capacitive current is observed. Thus, the ORR is controlled by charge transfer. In the second region, ranging from −0.1 to −0.5 V, the ORR is found to operate in a mixed regime; in other words, the reaction is controlled by both the charge transfer and the mass transport. In this range (between −0.1 and −0.5 V), an increase in the disk current causes a proportional increase in the ring current. Finally, in the third region, ranging between −0.5 and −0.8 V, the disk current presents a constant value; in other words, the reaction is controlled by mass transfer; and as such, it is limited by the amount of O_2 that reaches the disk via the diffusion process.

A comparison of the PCL6 electrode with that of the glassy carbon (GC) shows that, compared to the PCL6, the influence of current on the GC electrode is insignificant. For the PCL6, one will observe that the ORR onset shifted toward more positive potentials than observed in the case of the glassy carbon. The difference in terms of the shift in potential between the two electrodes was 400 mV. Thus, for the PCL6, the required potential and the energy consumption for ORR are found to be relatively lower compared to those of the glassy carbon. These findings are in agreement with

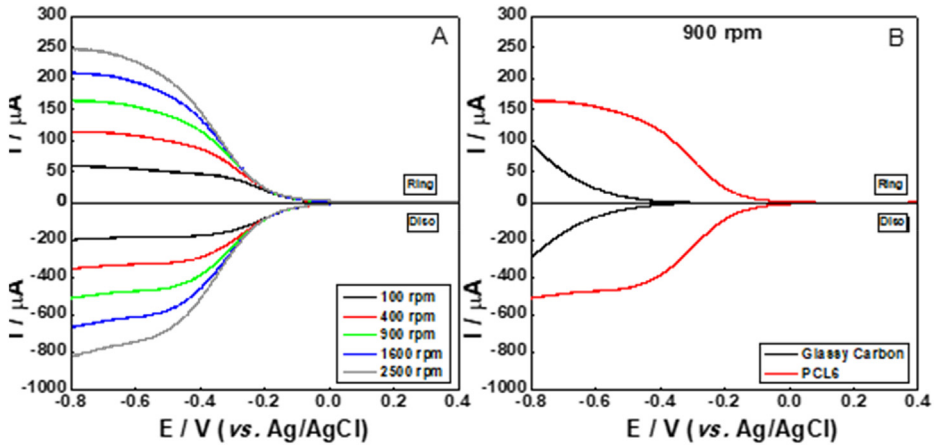

Fig. 4. Steady state polarization curves for ORR using RRDE system with PCL6 at different rotations (A) along with comparison between PCL6 and GC (B). The electrolyte employed was 0.1 mol L^{-1} K_2SO_4 at pH 2.0 saturated with O_2; the scan rate was 5 mVs^{-1}. (A colour version of this figure can be viewed online.)

those of the theoretical data, since the PCL6 sample presents a higher current value, with the reaction onset shifted to zero.

Carbon-based catalysts present a particularly complex surface structure [27]. Carbon edges are defined as heteroatom-free dopant which can change electronic structures of carbon materials. Graphite edges have been shown to possess higher activity towards ORR than basal plane. Moreover, the presence of edge-rich sites in dopant-free carbon nanomaterials can be increased by controlling treatment conditions, such as temperature and time [27]. As pointed out by L. Tao et al. [27], there may have been a possible increase in the number of edge-rich sites, and this contributed to the superior ORR performance on PCL6 film. Apart from the thermal treatment conducted on the PCL6 material prior to use, the observed shift in onset potential and higher current density are found to be strongly associated with carbon edge sites.

It is noteworthy that a previous study on PCL6 indicated I_D/I_G ratio of 1.84 [28]. This ratio is higher than the reported for graphene, and indicates the presence of higher concentration of defects on PCL6 surface, which possibly leads to the formation of edges and holes [27], as well as higher carbon concentration bonded to oxygenated functional groups [28]. Considering the hybridization status of carbon, the presence of double bonds (sp^2) facilitates the interaction of oxygen with the carbon surface. On the other hand, carbon materials with higher sp^3 content are characterized by an impeded adsorption, which leads to lower conductivity. Yeager [1] has described the possible interaction pathways for ORR. The Griffiths model is based on side-on lateral interactions of oxygen π orbitals. By contrast, the Pauling model is related to end-on lateral interactions and the Bridge model may occur by either side-on (cis) or end-on (trans) lateral interactions.

To better understand the mechanism involving adsorption, activation, reaction and mass transport, electrochemical impedance spectroscopy measurements were performed using several potentials. For data adjustment purposes, two equivalent circuits were used; this involved the use of the same circuit elements with only a slight alteration in their arrangements. R_{sol} is the resistance of the solution. To represent the electronic part of the processes, R_{ct} is the charge transfer and Q_{dl} is the double layer non-ideal capacitance, both lying in parallel with each other. The ionic part is described by the pair R_{mt} and Q_{mt}; these represent the resistance and pseudo-capacitance of the mass transport, respectively, with both lying in parallel to one another. To adjust the GC data, the pair R_{mt}/Q_{mt} is represented in series with the pair R_{ct}/Q_{dl}. With regard to PCL6, the R_{mt}/Q_{mt} pair is represented in parallel with R_{ct} and in series with Q_{dl}, a configuration widely used for porous electrodes [29] (Fig. 5). Although the parameters R_{mt} and Q_{mt} are related to mass transport, processes occurring slower than the charge transfer play an influential role on these parameters, since the time constant appears at lower frequencies. The models employed can be found in the inset of each Nyquist. In section I of the Supplementary Information, one will find the table with the values of the parameters, as well as the χ^2 of the fits.

Based on the impedance parameters as a function of the potential, one can offer a plausible explanation regarding the processes that take place in each sample. Fig. 6 shows the charge transfer resistance and the double layer capacitance for GC and PCL6. The linear voltammetry profile was also plotted in order to facilitate the association with the several transport regions. For direct comparison purposes, all the graphs are in the same scale.

In both samples, a significant decrease was observed in the charge transfer resistance as the potential applied was close to the potential of the peroxide formation. This is an expected behaviour, since the O_2 reduction reaction is associated with a mechanism in which O_2 adsorption requires a minimum energy to occur, *i.e.*, a minimal potential value. It is interesting to note that, the onset of the reaction in PCL6 occurs at the same time as the sudden drop in resistance observed on the electrode. In addition, the change in resistance is found to occur sooner than the decrease in current; this may imply that the electrode undergoes a period of activation prior to the beginning of the reaction, which is probably associated with the adsorption of O_2.

In this sense, the double layer capacitance appears to give a clearer idea about the changes on the electrode surface. Since the capacitance is proportional to the area, the observed variations can be associated with changes in the area itself. Thus, in both samples, one notices the occurrence of important changes at the same potentials, where a steady drop in resistance is observed. In the case of the GC, the capacitance value begins to drop at 0 V until it reaches the minimum value of −0.3 V; this implies that adsorption begins at around 0 V, while the reduction reaction begins after −0.3 V. As the product of the reduction does not remain adsorbed on the electrode, the electrode area available increases again. On the other hand, the capacitance profile indicates that, for PCL6, the adsorption occurs before 0.1 V due to the lower capacitance value, which begins to increase at −0.15 V (150 mV earlier than the GC). All these results are in agreement with the those observed in the quantum simulation. It is thermodynamically more favourable for O_2 to undergo adsorption on PCL6; in other words, less energy is required

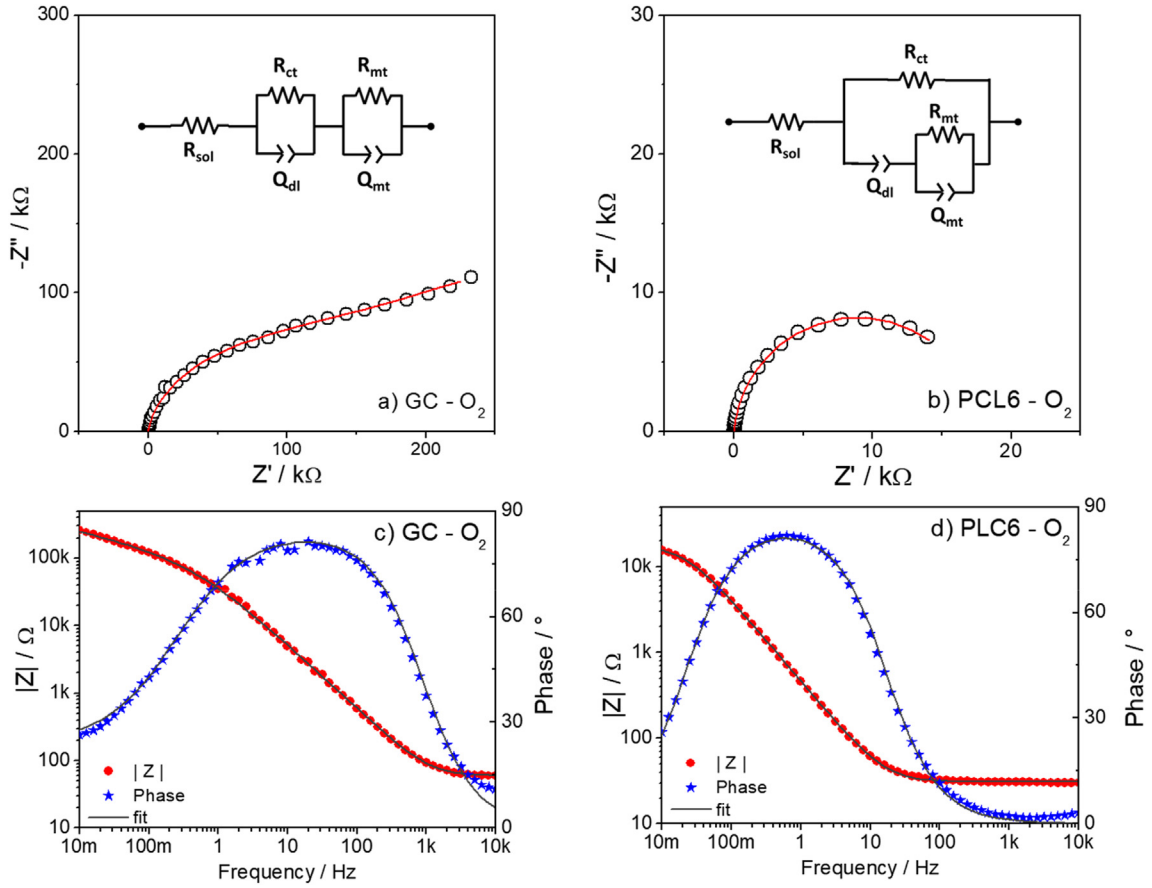

Fig. 5. Nyquist and equivalent circuits used to adjust the (A) GC and (B) PLC6 data. Bode Impedance Modulus and Bode Phase for (C) GC and (D) PLC6. The electrolyte was saturated with O_2, and the electrode was spun at 900 rpm. (A colour version of this figure can be viewed online.)

for the reaction to occur on PCL6 electrode. Moreover, since the weakening of the double bond is greater in this case, the formation of H_2O_2 will also demand less energy.

Concerning the transport of species, one can associate a slower time constant with this phenomenon. Fig. 7 shows some parameters that describe these dynamics. Despite being represented by circuit elements, these parameters should be interpreted in a less conventional way. Another point worth mentioning here has to do with the charge transport resistance. A high value of the charge transport resistance means that the transport occurs with greater intensity, whereas a smaller value indicates a lower flow of charges and/or charged species.

Generally, a decrease in charge transport resistance is observed as the potential shifts to more negative potentials; this is attributed to the saturation of adsorbed species in the active sites. The reaction kinetics controls the transport flow, since the reagent has to be converted into a product for a new site to be released. Unlike the GC electrode, in the case of the PCL6 electrode one observes an increase in the resistance value even after the potential of −0.4 V; this may be attributed to a rapid kinetic reaction which causes the products to be quickly formed. This inference is backed by the observation made earlier regarding time constant.

Finally, the kinetics of the reaction involving all the processes, from adsorption to product formation, is better visualized in the form of a constant. At the bottom of Fig. 7, one will find a representation of the charge transfer constant in relation to the potential. An analysis of the charge transfer constant enables one to understand the correlation between the afore-mentioned observations based on the voltammetries and EIS data regarding the steps of reaction. One will notice that there is a period of pre-activation of the electrode (species adsorption); this is followed by the onset of the reduction reaction at potentials smaller than expected, considering the current change in LSV.

From the potential of −0.3 V, a divergence of behaviour is observed between the GC and PCL6. A maximum value of charge transfer constant is observed for PCL6. However, this value begins to decline from −0.3 V onwards, indicating that from this potential onwards the reaction is solely controlled by mass transport. By contrast, the GC presents an ever-increasing value of charge transfer constant (although at a slower speed); this implies a kinetic control of the reaction rate. Although this pattern of behaviour is expected when one analyses the voltammetry profile, it appears to occur sooner than the current implies.

The results obtained from mechanical-quantum computations have also help to clarify the mechanism involving oxygen interaction with the surface. Considering that oxygen interacts more strongly with PCL6 surface, it is natural to observe a lower wattage of energy required for the reaction to occur (i.e., low potential values). On the other hand, the presence of more active sites on the surface, as evidenced by the calculations, explains the higher current density obtained for the GCE electrode modified with Printex.

4. Conclusions

The present study has confirmed the morphological and structural features of Printex L6 carbon black. This type of carbon is usually classified as nanomaterial composed of particle agglomerates with mean size of 30 nm. This information was confirmed in

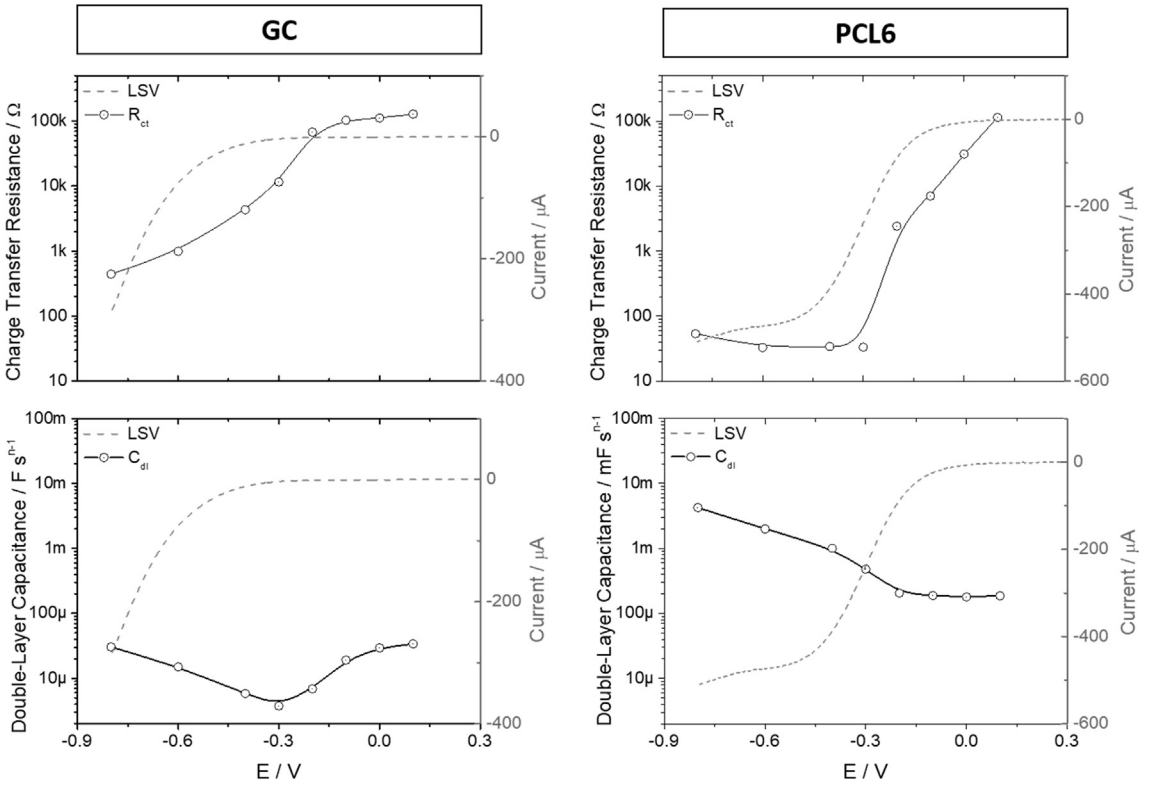

Fig. 6. Impedance parameters: charge transfer resistance and double layer capacitance in relation to applied potential and LSV curve at 900 rpm.

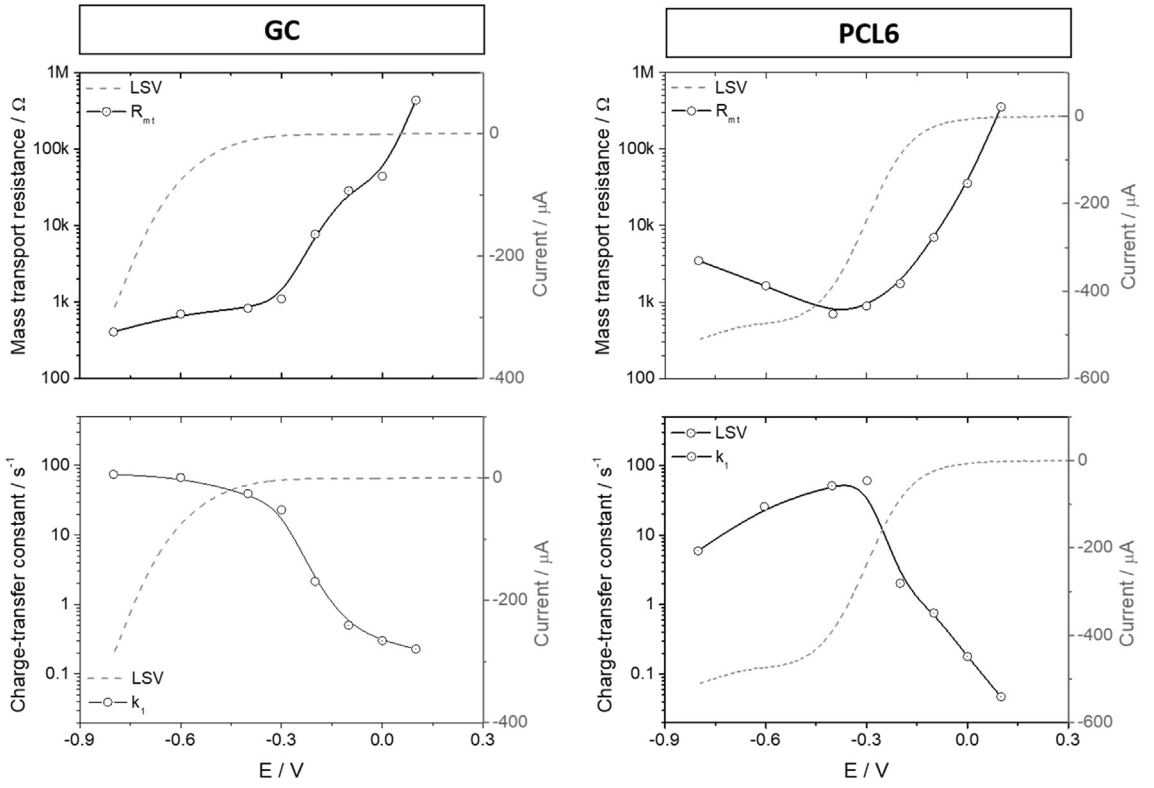

Fig. 7. Impedance parameters: mass transport resistance and charge transfer capacitance in relation to applied potential and LSV curve at 900 rpm.

the present study by SEM images and BET analyses. The results obtained in the investigation show that reduced particle size leads to the enhancement of surface area, in the order of 295 $m^2 g^{-1}$. In addition, PCL6 was found to be a highly porous material (with pore volume of 0.5 $cm^2 g^{-1}$). The presence of oxygenated groups and sp2 carbon on PCL6 surface contributed to an increase in the number of active sites, which led to a reduction of the diffusional energy barrier and improvement in the electron transfer rate on the electrode surface. Semi-empirical simulations indicated oxygen resonance interaction with carbon on PCL6 surface due to reduced equilibrium distance. This behaviour explains the increased catalytic effect commonly attributed to carbon black. A distinct local effect was also found to occur in the carbon lying close to oxygenated groups, mainly due to partial positive charge stabilization.

A causal relationship was also successfully established between electrochemical performance and PCL6 structure. Shifts in potential values toward more positive values were found to be related to higher density of active sites. The results obtained for capacitance were also correlated to impedimetric performance, where adsorption on PCL6 was found to begin at lower potential (150 mV), since the process was thermodynamically more favourable. The ionic contribution (R_{mt} and Q_{mt}) was found to be inversely related to charge transfer resistance in the presence of amorphous carbon. The charge transfer constant confirmed the existence of a pre-activation process which occurs before ORR, earlier than the current change implied. The first report of its kind, this study has been able to confirm patterns of electrochemical behaviour observed and described previously in the literature.

Acknowledgements

The authors acknowledge the financial support provided by the Brazilian funding agencies, which include the Brazilian National Council for Scientific and Technological Development - CNPq (grants no. 465571/2014-0, 301492/2013-1, 302874/2017-8 and 427452/2018-0), São Paulo Research Foundation (FAPESP – grants #2011/14314-1, #2014/50945-4, #2014/11861-0, #2016/19612-4, #2016/01937-4 and #2017/10118-0) and the Coordenação de Aperfeiçoamento de Pessoal de Nível Superior (CAPES – Finance Code 001).

Appendix A. Supplementary data

Supplementary data to this article can be found online at https://doi.org/10.1016/j.carbon.2019.09.036.

References

[1] E. Yeager, Dioxygen electrocatalysis: mechanisms in relation to catalyst structure, J. Mol. Catal. 38 (1986) 5–25, https://doi.org/10.1016/0304-5102(86)87045-6.
[2] E. Yeager, Electrocatalysts for O2 reduction, Electrochim. Acta 29 (1984) 1527–1537, https://doi.org/10.1016/0013-4686(84)85006-9.
[3] U.A. Paulus, T.J. Schmidt, H.A. Gasteiger, R.J. Behm, Oxygen reduction on a high-surface area Pt/Vulcan carbon catalyst: a thin-film rotating ring-disk electrode study, J. Electroanal. Chem. 495 (2001) 134–145, https://doi.org/10.1016/S0022-0728(00)00407-1.
[4] H.R. Colón-Mercado, B.N. Popov, Stability of platinum based alloy cathode catalysts in PEM fuel cells, J. Power Sources 155 (2006) 253–263, https://doi.org/10.1016/j.jpowsour.2005.05.011.
[5] Y. Ma, H. Wang, S. Ji, J. Goh, H. Feng, R. Wang, Highly active Vulcan carbon composite for oxygen reduction reaction in alkaline medium, Electrochim. Acta 133 (2014) 391–398, https://doi.org/10.1016/j.electacta.2014.04.080.
[6] C.M. Long, M.A. Nascarella, P.A. Valberg, Carbon black vs. black carbon and other airborne materials containing elemental carbon: physical and chemical distinctions, Environ. Pollut. 181 (2013) 271–286, https://doi.org/10.1016/j.envpol.2013.06.009.
[7] R.M. Reis, R.B. Valim, R.S. Rocha, A.S. Lima, P.S. Castro, M. Bertotti, M.R.V. Lanza, The use of copper and cobalt phthalocyanines as electrocatalysts for the oxygen reduction reaction in acid medium, Electrochim. Acta 139 (2014) 1–6, https://doi.org/10.1016/j.electacta.2014.07.003.
[8] M.H.M.T. Assumpção, R.F.B. De Souza, D.C. Rascio, J.C.M. Silva, M.L. Calegaro, I. Gaubeur, T.R.L.C. Paixão, P. Hammer, M.R.V. Lanza, M.C. Santos, A comparative study of the electrogeneration of hydrogen peroxide using Vulcan and Printex carbon supports, Carbon N. Y. 49 (2011) 2842–2851, https://doi.org/10.1016/j.carbon.2011.03.014.
[9] F. Wang, S. Hu, Studies of electrochemical reduction of dioxygen with RRDE, Electrochim. Acta 51 (2006) 4228–4235, https://doi.org/10.1016/j.electacta.2005.11.042.
[10] C. Chemistry, M. Modeling, Computational Chemistry and Molecular Modeling, 2008, https://doi.org/10.1007/978-3-540-77304-7.
[11] R.A. Sidik, A.B. Anderson, N.P. Subramanian, S.P. Kumaraguru, B.N. Popov, O2 reduction on graphite and nitrogen-doped graphite: experiment and theory, J. Phys. Chem. B 110 (2006) 1787–1793, https://doi.org/10.1021/jp055150g.
[12] J.F. Carneiro, L.C. Trevelin, A.S. Lima, G.N. Meloni, M. Bertotti, P. Hammer, R. Bertazzoli, M.R.V. Lanza, Synthesis and characterization of ZrO2/C as electrocatalyst for oxygen reduction to H2O2, Electrocatalysis 8 (2017) 189–195, https://doi.org/10.1007/s12678-017-0355-0.
[13] B. Ruiz-Camacho, J.C. Baltazar Vera, A. Medina-Ramírez, R. Fuentes-Ramírez, G. Carreño-Aguilera, EIS analysis of oxygen reduction reaction of Pt supported on different substrates, Int. J. Hydrogen Energy 42 (2017) 30364–30373, https://doi.org/10.1016/j.ijhydene.2017.08.087.
[14] B. Bera, T. Kar, A. Chakraborty, M. Neergat, Influence of nitrogen-doping in carbon on equivalent distributed resistance and capacitance – implications to electrocatalysis of oxygen reduction reaction, J. Electroanal. Chem. 805 (2017) 184–192, https://doi.org/10.1016/j.jelechem.2017.10.025.
[15] Z. Chen, H. Dong, H. Yu, H. Yu, In-situ electrochemical flue gas desulfurization via carbon black-based gas diffusion electrodes: performance, kinetics and mechanism, Chem. Eng. J. 307 (2017) 553–561, https://doi.org/10.1016/j.cej.2016.08.116.
[16] J.J.P. Stewart, Optimization of parameters for semiempirical methods IV: extension of MNDO, AM1 and PM3 to more main group elements, J. Mol. Model. 10 (2004) 155–164, https://doi.org/10.1007/s00894-004-0183-z.
[17] J.J.P. Stewart, Optimization of parameters for semiempirical methods VI: more modifications to the NDDO approximations and re-optimization of parameters, J. Mol. Model. 19 (2013) 1–32, https://doi.org/10.1007/s00894-012-1667-x.
[18] B.R. Brooks, C.L. B III, J.A.D. Mackerell, L. Nilsson, R.J. Petrella, B. Roux, Y. Won, G. Archontis, C. Bartels, S. Boresch, A. Caflisch, L. Caves, Q. Cui, A.R. Dinner, M. Feig, S. Fischer, J. Gao, M.W.I. Hodoscek, M. Karplus, CHARMM: the biomolecular simulation program B, J. Comput. Chem. 30 (2009) 1545–1614, https://doi.org/10.1002/jcc.
[19] A.A. Chen, R.V. Pappu, Parameters of monovalent ions in the AMBER-99 forcefield: assessment of inaccuracies and proposed improvements, J. Phys. Chem. B 111 (2007) 11884–11887, https://doi.org/10.1021/jp0765392.
[20] L. Verlet, Computer "experiments" on classical fluids. I. Thermodynamical properties of Lennard-Jones molecules, Phys. Rev. 159 (1967) 98–103, https://doi.org/10.1103/PhysRev.159.98.
[21] A. Klamt, G. Schüürmann, COSMO: a new approach to dielectric screening in solvents with explicit expressions for the screening energy and its gradient, J. Chem. Soc., Perkin Trans. 2 (1993) 799–805, https://doi.org/10.1039/P29930000799.
[22] A. Moraes, M.H.M.T. Assumpção, F.C. Simões, V.S. Antonin, M.R.V. Lanza, P. Hammer, M.C. Santos, Surface and catalytical effects on treated carbon materials for hydrogen peroxide electrogeneration, Electrocatalysis 7 (2016) 60–69, https://doi.org/10.1007/s12678-015-0279-5.
[23] L.A. Goulart, T.T. Guaraldo, M.R.V. Lanza, A novel electrochemical sensor based on Printex L6 carbon black carrying CuO/Cu2O nanoparticles for propylparaben determination, Electroanalysis 30 (2018) 2967–2976, https://doi.org/10.1002/elan.201800549.
[24] T.L. Cottrell, The Strengths of Chemical Bonds, second ed., Butterworths Scientific Publications, Butterworths, London, 1958.
[25] A. Nilsson, L.G.M. Pettersson, Adsorbate electronic structure and bonding on metal surfaces, Chem. Bond. Surfaces Interfaces (2008) 57–142, https://doi.org/10.1016/B978-044452837-7.50003-4.
[26] R. Fiengo, R. Fiengo, Surface Structure (1980) 1–56.
[27] L. Tao, Q. Wang, S. Dou, Z. Ma, J. Huo, S. Wang, L. Dai, Edge-rich and dopant-free graphene as a highly efficient metal-free electrocatalyst for the oxygen reduction reaction, Chem. Commun. 52 (2016) 2764–2767, https://doi.org/10.1039/c5cc09173j.
[28] T.T. Guaraldo, L.A. Goulart, F.C. Moraes, M.R.V. Lanza, Carbon black nanospheres modified with Cu (II)-phthalocyanine for electrochemical determination of Trimethoprim antibiotic, Appl. Surf. Sci. 470 (2019) 555–564, https://doi.org/10.1016/j.apsusc.2018.09.226.
[29] W. Kwon, J.M. Kim, S.W. Rhee, A new equivalent circuit model for porous carbon electrodes in charge transfer reaction of iodide/triiodide redox couples, Electrochim. Acta 68 (2012) 110–113, https://doi.org/10.1016/j.electacta.2012.02.056.